Journal of Fluorescence
https://doi.org/10.1007/s10895-023-03576-7

RESEARCH

Ethyl 3-aminobenzo[b]thiophene-2-carboxylate Derived Ratiometric Schiff Base Fluorescent Sensor for the Recognition of In^{3+} and Pb^{2+}

Shifeng Zhu[1] · Liangru Yang[1] · Yingying Zhao[1]

Received: 26 November 2023 / Accepted: 28 December 2023

Abstract

An ethyl 3-aminobenzo[b]thiophene-2-carboxylate derived ratiometric Schiff base fluorescent sensor **R** was devised and synthesized. **R** exhibited a highly sensitive and selective ratiometric response to In^{3+} in DMF/H_2O tris buffer solution. **R** exhibited a colorimetric/fluorescent dual-channel response to In^{3+}. More importantly, **R** can distinguish In^{3+} from Ga^{3+} and Al^{3+} in less than 5 min. **R** exhibited a good linear correlation with the concentration of In^{3+} in the 5–25 μM range and the limit of detection for In^{3+} was found to be 8.36×10^{-9} M. According to the job`s plot and MS spectra, **R** formed a complex with In^{3+} at 1:2 with a complexation constant of 8.24×10^{9} M^2. Based on Gaussian theory calculations, the response mechanism of **R** to In^{3+} can be explained by photo-induced electron transfer (PET) and intramolecular charge transfer (ICT) mechanisms. In addition, **R** can be used for the detection of indium in tap water with satisfactory recoveries. Meanwhile, **R** displayed a linear relationship to micromolar concentrations (0-50 μM) of Pb^{2+} and recognized Pb^{2+} in a ratiometric response with a detection limit of 8.3×10^{-9} M.

Keywords Benzo[b]thiophene · Ratiometric sensor · Schiff base · Indium

Introduction

Indium is a transition metal belonging to the third main group. Its content in the earth's crust is very small, only about one-sixth of gold. It is widely used in related fields such as liquid crystal display (LCD), semiconductor materials, and solar cells [1–4]. Due to the widespread use of indium, the harm caused by indium to the environment and human beings directly or indirectly cannot be underestimated [5, 6]. Recent research has revealed that indium is hazardous to people and animals, exhibiting carcinogenicity, embryotoxicity, and teratogenicity [7–9]. In addition, other studies have shown that indium may be interfering with iron metabolism and damage liver cells [10–12]. Therefore, synthesizing efficient and sensitive detection sensors for In^{3+} is of great significance. On the other hand, lead is one of the poisonous metal ions that widely exist in nature. Due to its low degradability and water solubility, lead usually exists in nature for a long time [13–16]. The use of lead seriously endangers human health and destroys natural ecosystems [17, 18]. Excessive lead can affect the human kidneys, stomach, blood, and nervous system, resulting in a variety of human diseases.

Metal ions have been monitored using traditional detection methods such as inductively coupled plasma mass spectrometry (ICP-MS), atomic absorption spectrometry (AAS), inductively coupled plasma atomic emission spectrometry (ICP-AES), and electrochemical methods, but these methods are expensive, time-consuming, and require professional operation [19–22]. In recent years, fluorescent sensors have been gradually replacing traditional detection methods with simple operation, low cost, and rapid response, and have become a new technology widely used for detecting metal ions [23–27]. As a commercial fluorescent sensor, Schiff base has received increasing attention due to its unique ability to recognize metals and its one-step synthesis process [28, 29]. Among them, Schiff base chemical sensors based on thiophene and its derivatives are widely used in the detection of metal ions, anions, and amino acids [30–35].

The use of strong fluorophores is required to guarantee that Schiff base sensors operate well. In addition, molecules containing push–pull electron groups are highly fluorescent due to intramolecular charge transfer from the donor

✉ Yingying Zhao
zhaoyy@haut.edu.cn

[1] College of Chemistry and Chemical Engineering, Henan University of Technology, Zhengzhou 450001, China

Published online: 11 January 2024

group to the acceptor group. Consequently, we present 3-aminobenzo[b]thiophene as a novel chromophore system in which the appropriate structure promotes intramolecular charge transfer (ICT). Scattered reports with benzo[b]thiophene based chemosensors are documented for Fe^{3+}, F^-, CN^-, and OH^- ions [36–38]. As far as we know, this is the first publication to systematically investigate the ability of 3-amino-benzo[b]thiophene as a ratio sensor to detect indium ions. On the other hand, it is well known that single-channel emission intensity measurements are often influenced by factors such as ambient temperature, solution polarity, and instrument efficiency [39]. On the contrary, ratiometric fluorescent sensors respond to the detection effect by the intensity ratio of two emission wavelengths, which can eliminate the influence of the above factors and thus improve the accuracy of detection [40].

Now, we designed and synthesized a new benzo[b]thiophene-based bifunctional Schiff base sensor **R**, which distinguished In^{3+} from Al^{3+} and Ga^{3+} with a relatively low detection limit. The addition of In^{3+} ions caused the solution to change from colorless to yellow and the fluorescence color to change from colorless to green. What`s more, **R** can be used for the quantitative detection of In^{3+} in tap water. At the same time, we found that Pb^{2+} caused a large red-shift in the emission spectrum of **R**.

Experimental Section

Sample Preparation

All chemicals were analytically pure and not treated before use; all metal cations ($AgNO_3$, $CrCl_3$, $FeCl_3$, $FeCl_2$, $CoCl_2$, $ZnCl_2$, $AlCl_3$, KCl, $CdCl_2$, $NiCl_2$, $GaCl_3$, NaCl, $MgCl_2$, $InCl_3$, $CaCl_2$, $CuCl_2$, $BaCl_2$, $HgCl_2$, $MnCl_2$, LiCl, $ZrCl_4$, $SnCl_2$, $Pb(NO_3)_2$) stock solution prepared by deionized water unified into 0.01 M. Sensor **R** was best soluble in DMF; water was added to exclude water from interfering with **R** selectivity. Considering the solubility of the sensor **R**, the stock solution of **R** was prepared with DMF/H_2O tris buffer (v/v, 9:1, 10 mM, pH 7.4).

Measurements

Fluorescence data and UV–vis spectra were obtained by fluorescence spectrometer F-7000 and Shimadzu UV–visible spectrophotometer UV-2600, respectively. The fluorescence spectrum was measured at an excitation wavelength of 275 nm, and both the excitation and emission slits were 5 nm. ^{1}H NMR spectra was obtained from Bruker 500 MHz AVANCE III spectrometer using tetramethylsilane (TMS) as an internal standard and DMSO-d_6 as the solvent. Infrared spectra were obtained using a WQF-530 FT-IR spectrometer with KBr pellets. All reaction processes were monitored by TLC (thin layer chromatography).

Job's Plot

Sensor **R** (1×10^{-4} M) stock solution and blank solution in DMF/H_2O (v/v, 9:1, 10 mM, pH 7.4) were prepared. Then **R** stock solution 1, 2, 3…8, and 9 mL were placed in nine vials and diluted to 10 mL with a blank solution. the solution was configured to 1×10^{-5} M, 2×10^{-5} M, 3×10^{-5} M…8×10^{-5} M, and 9×10^{-5} M sensor solution. Then 3 mL diluted **R** solution was taken, and a certain amount of In^{3+} ion solution was added to each to get the sum of sensor concentration and ion concentration to 1×10^{-4} M. Each solution was measured for its fluorescence spectrum by placing it in a cuvette.

Synthesis of Sensor R

Compound **1** (Ethyl 3-aminobenzo[b]thiophene-2-carboxylate) and compound **2** (3-aminobenzo[b]thiophene-2-carbohydrazide) were synthesized according to the methods that have been previously reported in the literature [41].

(E)-3-amino-N`-(2-hydroxybenzylidene) benzo[b] thiophene-2-carbohydrazide (**R**) was synthesized via the synthetic route in Scheme 1. The compound **2** (0.0518 g, 0.25 mmol) and salicylaldehyde (0.0794 g, 0.65 mmol) were mixed in ethanol solution and refluxed for four hours. After the solution was cooled to room temperature, it was filtered under reduced pressure and dried naturally to give a yellow powdery solid. 0.044 g, yield 59.59%. Elemental analysis: calculated for $C_{16}H_{13}N_3O_2S$, calculated: C, 62.154; H, 3.672; N, 13.552; O, 10.366; S, 10.236%. ^{1}H NMR (500 MHz, DMSO-d_6) δ 11.40 (s, 1H), 8.43 (s, 1H), 8.13 (d, $J=8.1$ Hz, 1H), 7.87 (d, $J=8.1$ Hz, 1H), 7.60 (s, 1H), 7.50 (t, $J=7.6$ Hz, 1H), 7.39 (t, $J=7.5$ Hz, 1H), 7.26 (t, $J=7.7$ Hz, 1H), 6.98–6.89 (m, 2H). ^{13}C NMR (126 MHz, DMSO) δ 166.29, 157.04, 151.83, 141.91, 139.29, 131.44, 128.71, 126.94, 124.23, 123.33, 123.12, 121.24, 120.03, 116.76, 94.79. FT-IR (KBr, cm^{-1}): $\nu=3101$ (CONH), 1843 (C=O), 1574 (C=N), 1439 (C-N). ESI–MS: $m/z=312.0802$ $[M+H]^+$.

Results and Discussion

The dual-effect sensor **R** was synthesized through the synthetic route in Scheme 1. Based on ^{1}H NMR, ^{13}C NMR, FT-IR and MS spectra, the molecular structure of **R** was consistent with the experimental part (Figs. S1–S4). Sensor **R** provides multiple oxygen and nitrogen atoms as binding sites and is expected to coordinate with metal ions to form stable complexes.

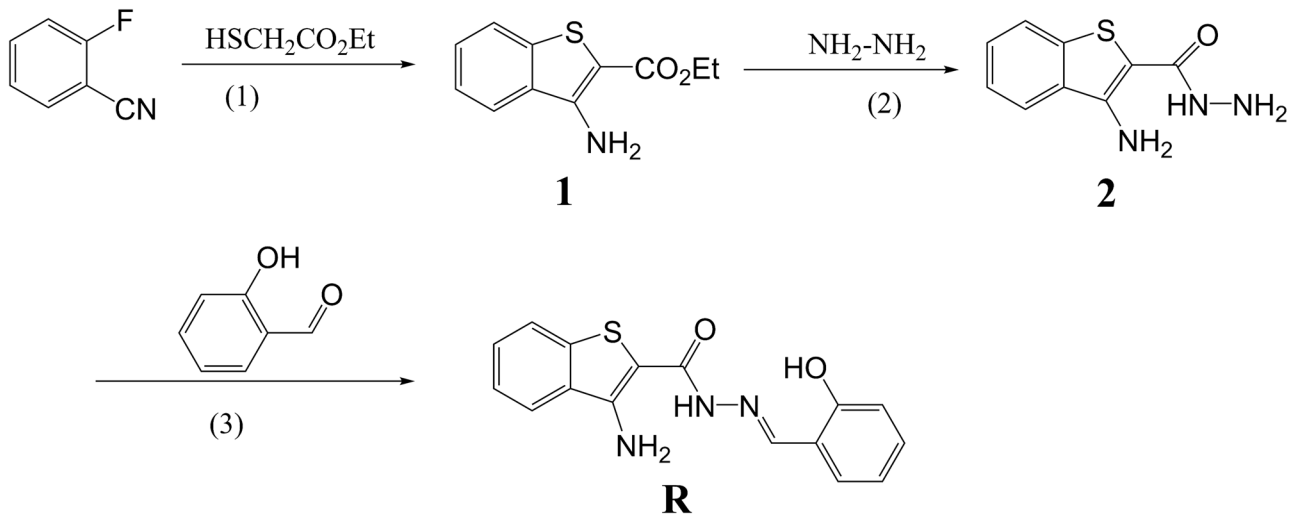

Scheme 1 Synthetic route of **R**. Conditions: (1) DMSO, NEt_3, reflux, 100 ℃, 3 h; (2) ethanol, reflux, 9 h; (3) ethanol, reflux, 4 h

Spectroscopic Studies of R to In^{3+}

Selectivity of R to In^{3+}

To evaluate the selectivity of sensor **R** to metal ions, various metal ions ($AgNO_3$, $CrCl_3$, $FeCl_3$, $FeCl_2$, $CoCl_2$, $ZnCl_2$, $AlCl_3$, KCl, $CdCl_2$, $NiCl_2$, $GaCl_3$, NaCl, $MgCl_2$, $InCl_3$, $CaCl_2$, $CuCl_2$, $BaCl_2$, $HgCl_2$, $MnCl_2$, LiCl, $ZrCl_4$, $SnCl_2$, $Pb(NO_3)_2$) were added to DMF/H_2O tris buffer solution (v/v, 9:1, 10 mM, pH 7.4). As shown in Fig. 1(a) and (b), free **R** showed weak fluorescence at 420 nm. The fluorescence spectrum was modified in the long-wave direction by In^{3+}, Al^{3+}, and Ga^{3+}, but only In^{3+} was able to cause a significant fluorescence ratio response and showed a color change. The addition of In^{3+} caused the solution to become yellow and caused the fluorescence emission of **R** to shift from 420 to 480 nm. Surprisingly, fluorescence emission was red-shifted from 420 to 525 nm when only Pb^{2+} was present, suggesting that **R** also has the potential to detect Pb^{2+}. The fluorescent color change was shown in Fig. 1(c), the fluorescent color of the solution changed from colorless to green only after the addition of In^{3+}, while the other cations remained unchanged. From the fluorescence data, it was clear that **R** can be used as an efficient colorimetric ratio measurement sensor for In^{3+}. In particular, it can be distinguished from the cognate elements Al^{3+} and Ga^{3+}.

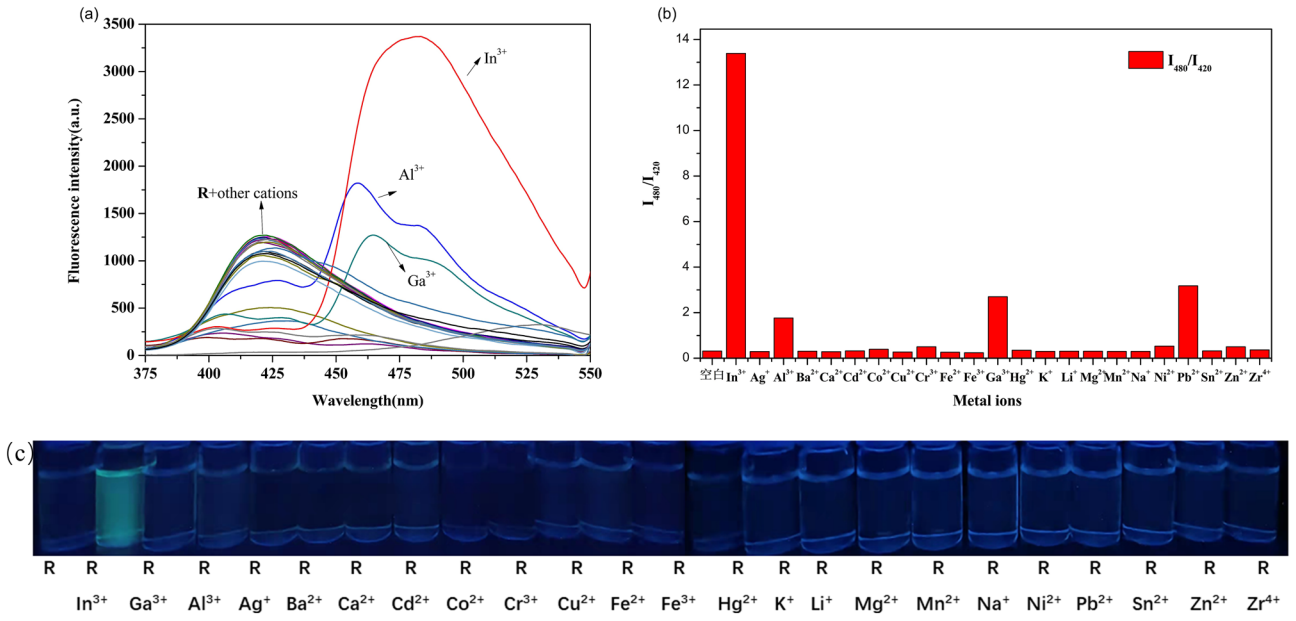

Fig. 1 **a** and **b** Selectivity of **R** (5×10^{-5} M) in the presence of various metal ions (2 equiv.). **c** Fluorescence color change under 365 nm UV light

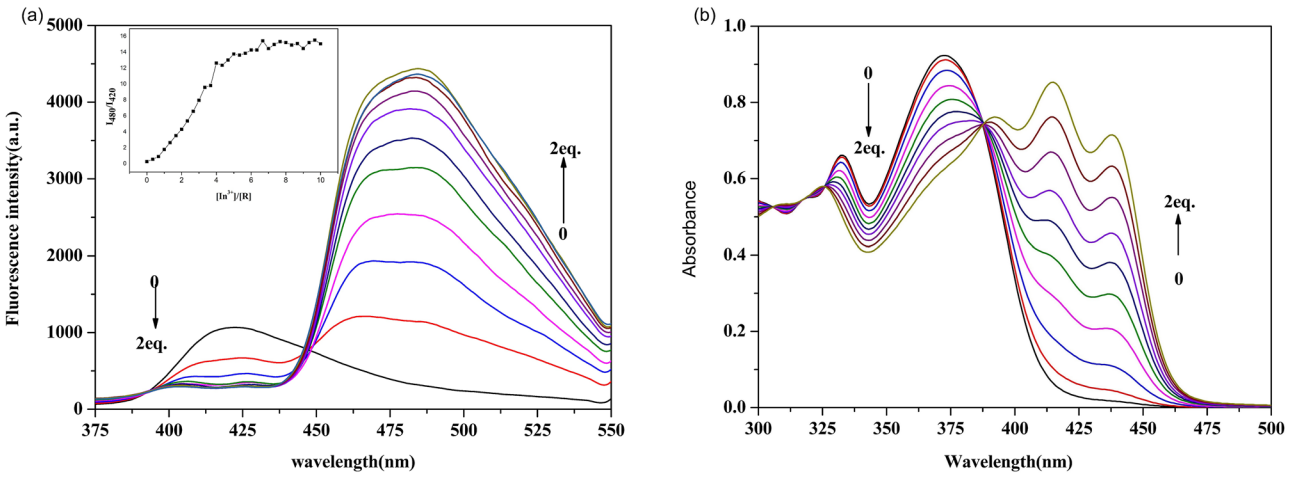

Fig. 2 **a** Fluorescence titration spectra of **R** (5×10^{-5} M) with the addition of In^{3+} (0–2 equiv.). Inset: change of the fluorescence intensity ratio (I_{480nm}/I_{420nm}). **b** Changes in the absorption spectrum of **R** (5×10^{-5} M) with the incremental addition of In^{3+} (0–2 equiv.) in DMF/H_2O tris buffer solution (v/v, 9:1, 10 mM, pH 7.4)

Photophysical Properties of R to In^{3+}

To investigate the photophysical properties of sensor **R** for In^{3+}, the fluorescence and UV–vis titration experiments were carried out in DMF/H_2O tris buffer solution (v/v, 9:1, 10 mM, pH 7.4). As can be seen from Fig. 2(a), the addition of In^{3+} (0–2 equiv.) resulted in a gradual decrease in fluorescence emission intensity at 420 nm and a gradual increase at 480 nm. With the increase of In^{3+} concentration, the emission intensity ratio (I_{480nm}/I_{420nm}) gradually increased (Fig. 2(a) insert). Furthermore, as shown in Fig. S5, the emission intensity ratio (I_{480nm}/I_{420nm}) of **R** exhibited a good linear correlation with the In^{3+} concentration in the 5 to 25 μM range, indicating that **R** can quantitatively analyze and detect In^{3+}. Through the corresponding linear equations $y=2.7653x-0.9748$ ($R^2=0.9978$), the LOD of In^{3+} was calculated to be 8.36×10^{-9} M based on the formula $LOD=3\sigma/S$, and the detection limit was lower than those of previously reported sensors (Table S3). Furthermore, according to the Benesi-Hildebrand equation, the association constant of the sensor **R**-In^{3+} complex was 8.24×10^{9} M^2 (Fig. S6), indicating that the sensor had a good complexation ability to In^{3+}. In addition, the UV–Vis spectrum showed that the absorption band of **R** was about 375 nm, and the absorption bands at 420 nm and 445 nm gradually increased with the increase of In^{3+} (0–2 equiv.). The occurrence of new absorption peak at 420 nm may be due to charge transfer jump and d-d* jump in the ligand field perturbation. A distinct isochromatic spot was observed at 388 nm, indicating that **R** combined with In^{3+} to form a stable complex.

Competition Study of R to In^{3+}

In addition, the competitive experiment was carried out to verify the selectivity of **R** for In^{3+} in the presence of competing metal ions (Ag^+, Al^{3+}, Ba^{2+}, Ca^{2+}, Cd^{2+}, Co^{2+}, Cr^{3+}, Cu^{2+}, Fe^{3+}, Ga^{3+}, Hg^{2+}, In^{3+}, K^+, Li^+, Mg^{2+}, Mn^{2+}, Na^+, Ni^{2+}, Pb^{2+}, Sn^{2+}, Zn^{2+}, Zr^{4+}) in DMF/H_2O tris buffer solution (v/v, 9:1, 10 mM, pH 7.4). The emission intensity of **R** was recorded after the addition of In^{3+} (2 equiv.) containing the other cations (Fig. 3). The fluorescence intensity of Co^{2+}, Cr^{3+}, Cu^{2+}, and Fe^{3+} were attenuated due to their strong quenching mechanism. However, the fluorescence of the **R**-In^{3+} was still evident in the presence of Co^{2+}, Cr^{3+}, Cu^{2+}, and Fe^{3+}. These results indicated that **R** has high selective sensing for In^{3+} ions and can distinguish In^{3+} ions from common interfering metal ions.

The Response Time and pH Range Study of R to In^{3+}

The reaction time determines the usefulness of the sensor for detection in real samples. Therefore, the time-dependent response of **R** toward In^{3+} was studied in DMF/H_2O tris buffer solution (v/v, 9:1, 10 mM, pH 7.4). As depicted in Fig. S7, the complexation of **R** with In^{3+} was completed within a few seconds, and the rapid reaction indicated that **R** could be used for the detection of In^{3+} in real samples.

It is important to note that one of the most basic and relevant parameters for chemosensor performance is pH. To gain an optimal pH range for monitoring In^{3+}, the fluorescence intensity changes of **R** in a series of DMF/H_2O solutions (v/v, 9:1, 10 mM) at pH 2–13 were studied. As displayed in Fig. S8, the fluorescence signal of **R** did not change significantly within the wide range of pH 2–13. As for **R**-In^{3+}, the emission intensity of **R**-In^{3+} was essentially unchanged at pH values below 5. This may be due to the protonation of the sensor at acidic pH. And then, the emission intensity ratio (I_{480nm}/I_{420nm}) significantly enhanced at pH ranged between

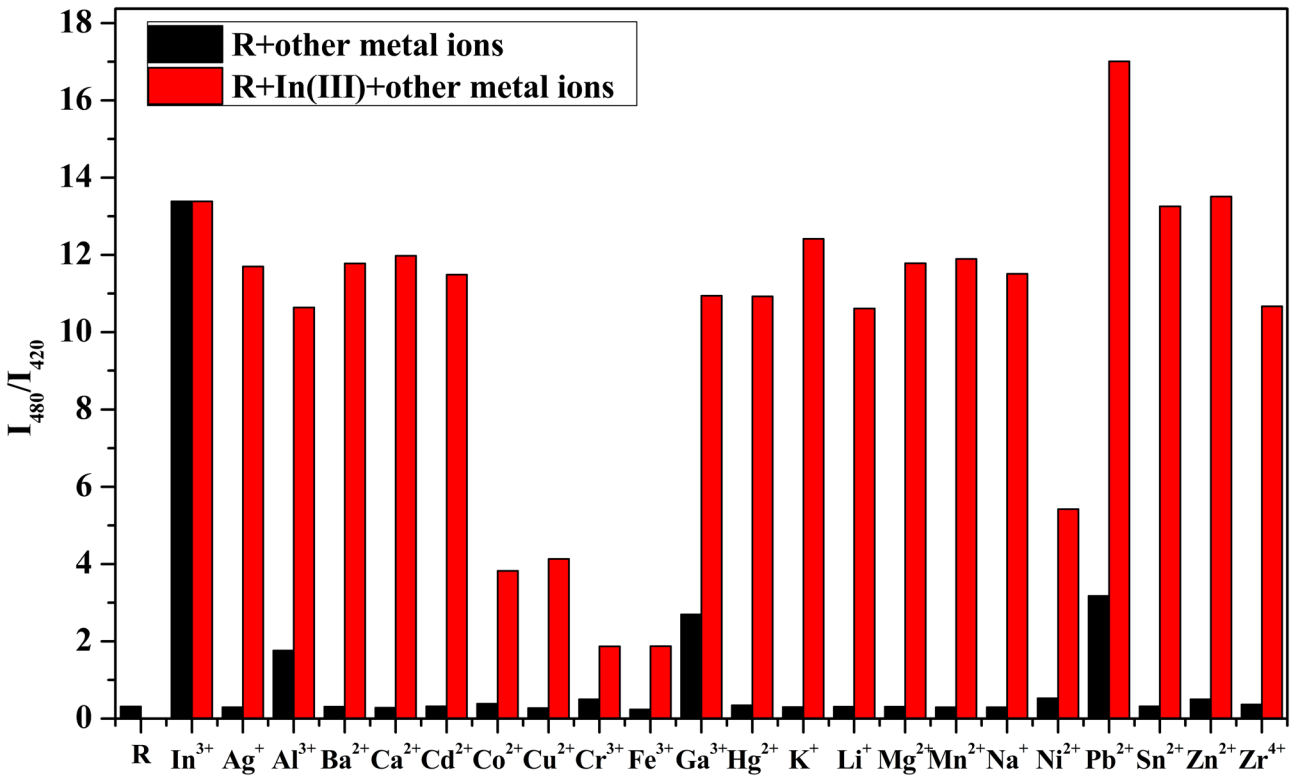

Fig. 3 Fluorescence intensity ratio (I_{480nm}/I_{420nm}) of **R** (5×10^{-5} M) towards In^{3+} (2 equiv.) in the presence of various other metal ions (2 equiv.) in DMF/H_2O tris buffer solution (v/v, 9:1, 10 mM, pH 7.4)

6 and 12. Therefore, **R** has a strong detection capability for In^{3+} at physiological pH.

Spectroscopic Studies of R to Pb^{2+}

When studying the selectivity of **R** to metal ions, we found that the addition of Pb^{2+} can observe a highly selective fluorescent ratio response, which prompted us to explore the fluorescence response of **R** to Pb^{2+}. The relevant tests were operated in the same buffer system. When treating solutions with different metal ions (Ag^{+}, Al^{3+}, Ba^{2+}, Ca^{2+}, Cd^{2+}, Co^{2+}, Cr^{3+}, Cu^{2+}, Fe^{2+}, Fe^{3+}, Ga^{3+}, Hg^{2+}, In^{3+}, K^{+}, Li^{+}, Mg^{2+}, Mn^{2+}, Na^{+}, Ni^{2+}, Pb^{2+}, Sn^{2+}, Zn^{2+}, Zr^{4+}), fluorescence emission was red-shifted from 420 to 525 nm when only Pb^{2+} was present, while other cations did not change significantly (Fig. 4).

To further study the photophysical properties of sensor **R** to Pb^{2+}, fluorescence and UV–vis titration experiments were carried out. The fluorescence titration experiment (Fig. 5(a)) depicted that **R** showed weak fluorescence at 420 nm under 275 nm excitation. After adding Pb^{2+} (0–3 equiv.), the fluorescence intensity at 420 nm decreased with increasing Pb^{2+} concentration and increased at 525 nm, thus the emission intensity ratio (I_{525nm}/I_{420nm}) increased (as illustrated in Fig. 5(a)) and reached a peak at 3 equiv. concentrations. As shown in Fig. 5(b), the absorption band of **R** was around 375 nm, as the concentration of Pb^{2+} (0–3 equiv.) in the solution of sensor **R** increased, the absorption band at 425 nm gradually increased, accompanied by a change in solution from colorless to yellow (Fig. 5(b) inset). There was a clear isochromatic point at 386 nm, indicating that **R** binds to Pb^{2+} to form a complex. The parameters were calculated based on the titration experimental data. The fluorescence emission intensity ratio and the concentration of Pb^{2+} showed a good linear relationship in the lower concentration range (Fig. 6(a)). By linear fitting, the relationship between the fluorescence emission intensity ratio and the concentration of Pb^{2+}, the detection limit (LOD) of Pb^{2+} was calculated to be 8.3×10^{-9} M.

Competition experiments were carried out to investigate the resistance of **R** to detect Pb^{2+} in the presence of three equal competing cations (Ag^{+}, Al^{3+}, Ba^{2+}, Ca^{2+}, Cd^{2+}, Co^{2+}, Cr^{3+}, Cu^{2+}, Fe^{2+}, Fe^{3+}, Ga^{3+}, Hg^{2+}, In^{3+}, K^{+}, Li^{+}, Mg^{2+}, Mn^{2+}, Na^{+}, Ni^{2+}, Pb^{2+}, Sn^{2+}, Zn^{2+}, Zr^{4+}). As shown in Fig. 6(b), the fluorescence intensity of **R**-Pb^{2+} was not affected by most metal ions except $Fe^{2+}$and Fe^{3+} having quenching properties [29]. While, the fluorescence of **R**-Pb^{2+} could still be observed despite the decrease in efficiency, indicating that **R** presented a strong anti-interference

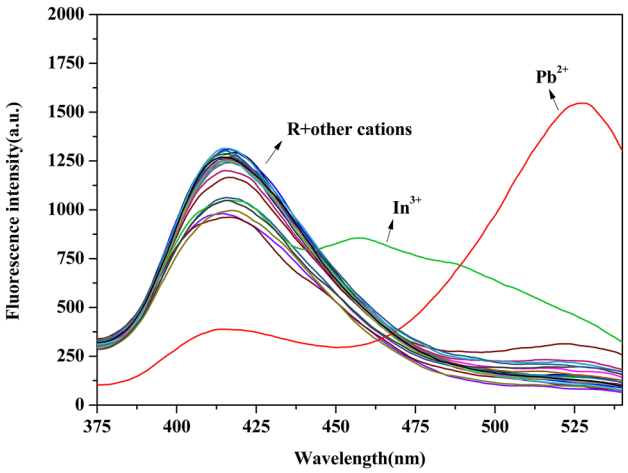

Fig. 4 Selectivity of **R** (1×10^{-5} M) in the presence of various metal ions (3 equiv.) in DMF/H_2O tris buffer solution (v/v, 9:1, 10 mM, pH 7.4)

against the other metal ions. What`s more, the In^{3+} signal was strong because In^{3+} enable a more complete quenching of the emission intensity of sensor **R** at 420 nm, and thus the emission intensity was stronger than the I_{525nm}/I_{420nm} signal when In^{3+} coexisted. Therefore, as mentioned above, **R** was remarkably selective for Pb^{2+} even when coexisting with other cations.

The Mechanism of Binding Mode

The formation of the new complex **R**-In^{3+} was determined based on the job`s plot. The fluorescence emission intensity ratio (I_{480nm}/I_{420nm}) showed the highest value at about 0.3 mol fraction (Fig. S9), indicating that the **R**-In^{3+} complex had a stoichiometric ratio of 1:2. Besides, the ESI–MS measurements were executed further to verify the formation of the complex, the obvious characteristic peak at m/z 677.0722 in Fig. S10 corresponding to [**R** + $2In^{3+}$-$3H^+$ + $4Cl^-$] with a 1:2 mode once more. Moreover, as displayed in the ^1H NMR titration spectra (Fig. S11), the chemical shifts of hydroxyl (-OH) groups around 10 ppm and amides (-NH-) around 11–12 ppm almost disappeared. The changes demonstrated that the addition of In^{3+} deprotonated the OH groups and underwent a ketone to enol structural change, resulting in coordination between the sensor **R** and In^{3+}.

As illustrated in Scheme 2, the possible binding mode of **R** and **R**-In^{3+} was proposed. The nitrogen atom of the C = N and the oxygen atoms of the hydroxyl group and carbonyl group were involved in the chelation of metal ions. The free **R** exhibited feeble fluorescence, and upon binding with In^{3+}, red-shift and fluorescence enhancement were observed in the emission spectra, which could be attributed to the following three reasons: (1) The red-shift of the emission spectrum of the sensor could be explained by the ICT mechanism [42]. Briefly, in the sensor **R**, photoinduction caused the electron transfer from the nitrogen atom of the imine structure to the benzo[b]thiophene ring; whereas in the complex **R**-In^{3+}, the electron transfer was blocked, which led to the red-shift of the spectrum. (2) The sensor **R** exhibited weak fluorescence due to the photo-induced electron transfer (PET) process caused by nitrogen atoms containing lone pair of electrons [43]; upon complexation with In^{3+}, the PET process was blocked, and in turn, the sensor exhibited significant fluorescence enhancement. (3) The free rotation of C = N in sensor **R** allowed it to emit weak fluorescence; however, the formation of complex **R**-In^{3+} restricted the free rotation of C = N

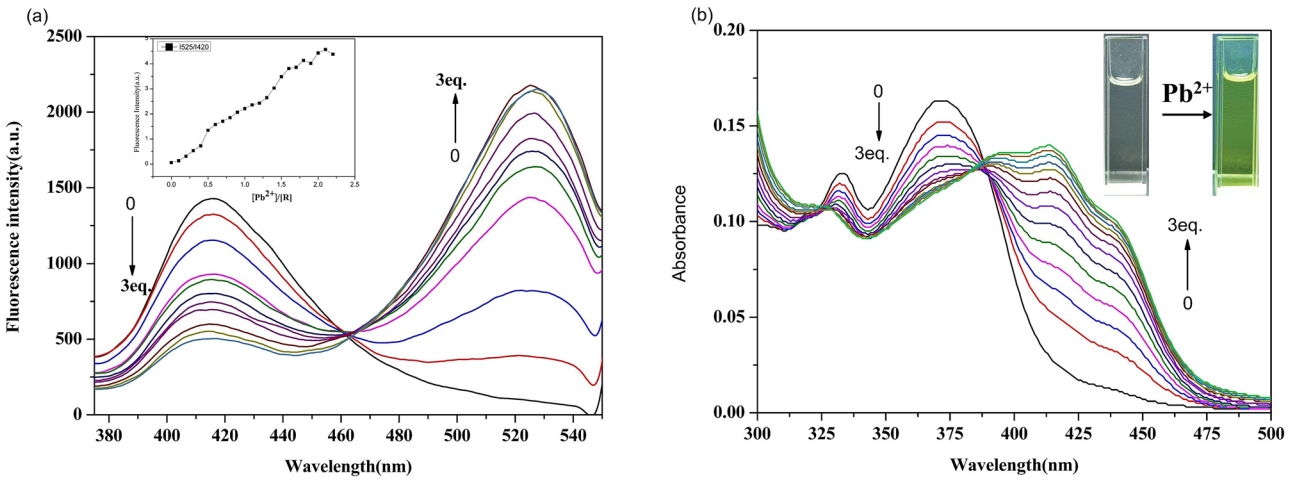

Fig. 5 **a** Fluorescence titration spectra of **R** (1×10^{-5} M) with the addition of Pb^{2+} (0–3 equiv.). Inset: change of the fluorescence intensity ratio (I_{525nm}/I_{420nm}). **b** Absorbance titration spectrum of **R** (1×10^{-5} M) with the incremental addition of Pb^{2+} (0–3 equiv.) in DMF/H_2O tris buffer solution (v/v, 9:1, 10 mM, pH 7.4)

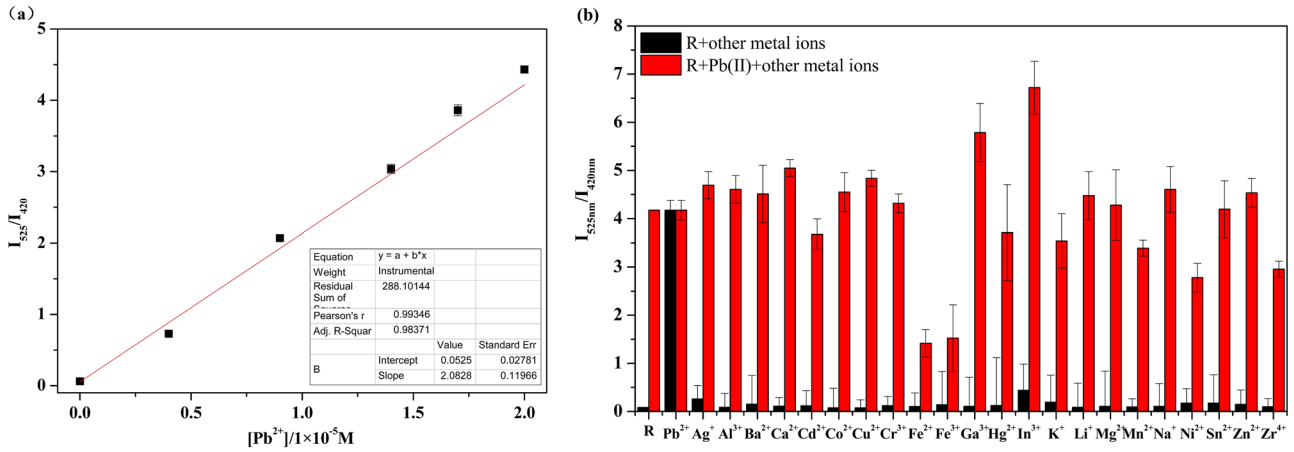

Fig. 6 **a** Fluorescence intensity ratio (I_{525nm}/I_{420nm}) of **R** (1×10^{-5} M) with the addition of Pb^{2+}. **b** Fluorescence intensity ratio (I_{525nm}/I_{420nm}) of **R** (1×10^{-5} M) towards Pb^{2+} (3 equiv.) in the presence of various other metal ions (3 equiv.) in DMF/H_2O tris buffer solution (v/v, 9:1, 10 mM, pH 7.4)

enhancing the fluorescent properties [44]. In addition, in the presence of EDTA, the complex **R**-In^{3+} is destroyed because the chelator EDTA is more capable of complexing with the metal ions, thus allowing the complex to be reversed.

To gain an understanding of the mechanism of **R** sensing of In^{3+}, the structural optimization and energy calculations were executed and analyzed using the Gaussian 09 program base on B3LYP/3-21G*. Figure 7 illustrated the optimized structure of **R** and **R**-In^{3+}. For the free sensor **R**, 3-aminobenzo[b]thiophene and salicylaldehyde exhibited an almost coplanarity. After complexing with In^{3+}, **R**-In^{3+} remained a good planar structure. Apparently, In^{3+} ions were imbedded into their coplanar structures through the dual chelating sites, which will result in the complexes with better rigidity and stability. On the other hand, in order to verify the hypothesis of the sensing mechanism, the electronic distributions of the sensors and complexes as well as the energy gaps of the HOMO (highest occupied molecular orbital) and the LOMO (lowest unoccupied molecular orbital) have also been determined (Fig. S12). The electron densities on the HOMO and LOMO of **R** were distributed on the units of salicylaldehyde and 3-aminobenzo[b]thiophene, indicating that the excited electrons will be transferred. Thus, the non-fluorescence of **R** was consistent with the PET mechanism. Besides, the HOMO-LOMO energy gap of **R** was calculated to be 3.8791 eV, while **R**-In^{3+} presented a reduced energy gap of 3.4004 eV. The narrower HOMO-LOMO energy gap suggested that the **R**-In^{3+} complex is more stabilized than the free **R**. The energy gap between the HOMO and LOMO orbitals decreased, which was consistent with the red shift of the spectrum and the ICT mechanism.

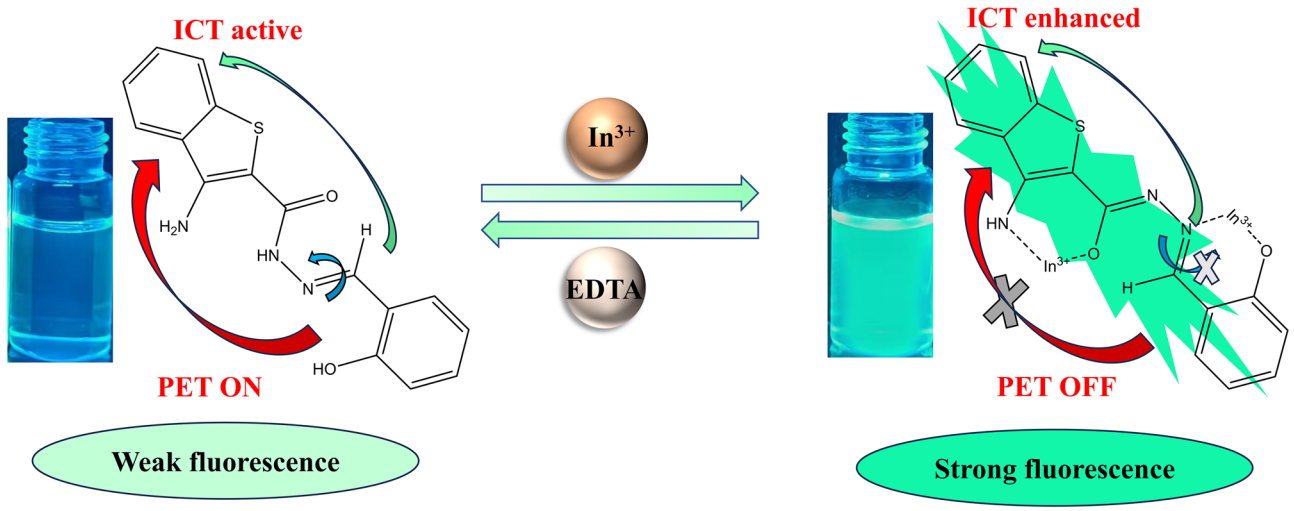

Scheme 2 The proposed binding mode of sensor **R** with In^{3+}

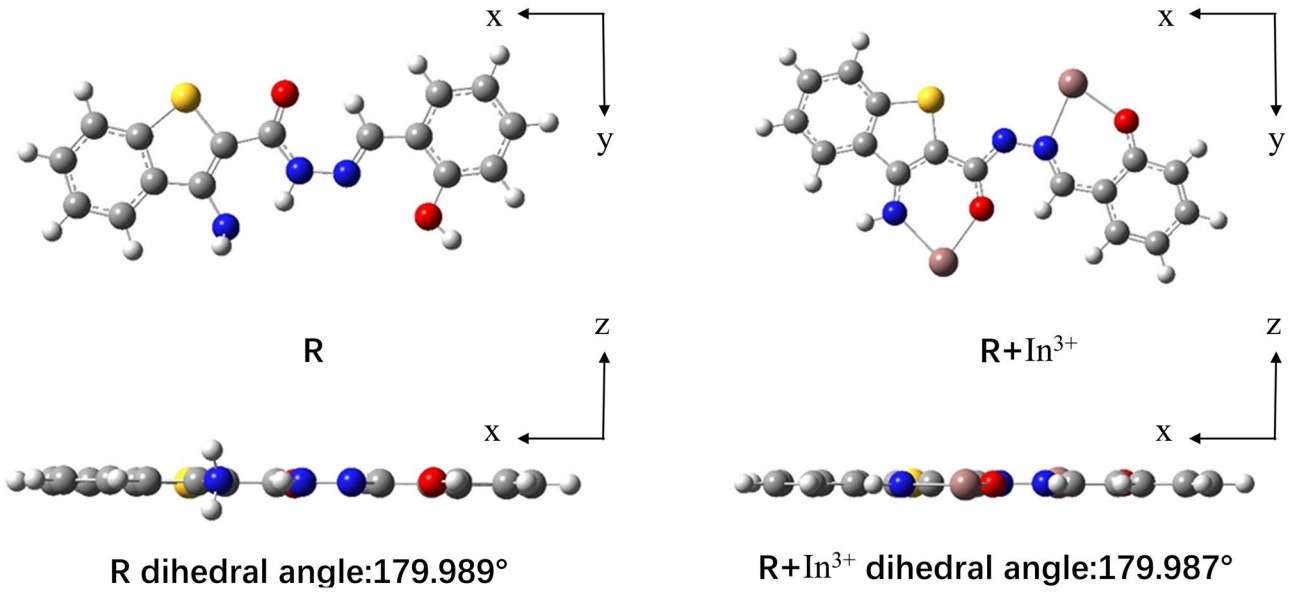

Fig. 7 The possible binding modes for **R** and R-In^{3+}

Based on the Multiwfn software [45], the electrostatic potentials on the surface of the molecule were utilized to detect the recognition process of the sensor and the target ions. The red and blue regions represent the positive and negative trends of the electrostatic potentials, respectively. As shown in Fig. S13, the negative potential area of sensor **R** was mainly concentrated in the binding site and salicylaldehyde site, and the positive potential area increased after binding with indium ion, indicating that sensor **R** formed a stable complex with indium ion.

Potential Application of R to In^{3+} Ions

Reversible Sensing Nature

Reversibility was another important property for sensors. Therefore, reverse experiments were performed on **R** using EDTA as the reverse reagent. As shown in Fig. 8, sensor **R** exhibited the maximum emission intensity at 420 nm. With the addition of In^{3+}, the emission intensity at 420 nm was weakened and enhanced at 480 nm. Then with the addition

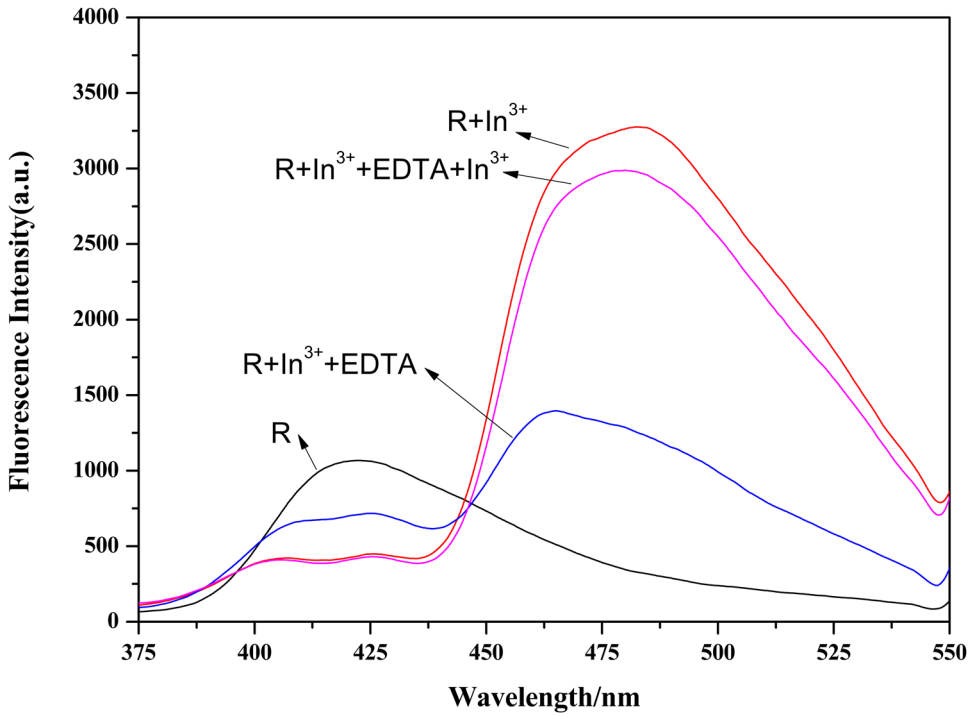

Fig. 8 The fluorescence emission spectra of free **R** and the **R**-In^{3+} system in absence and presence of EDTA

of EDTA, the emission intensity of **R**-In^{3+} diminished and the emission intensity of **R** at 420 nm recovered, ignoring the partial loss of fluorescence. This was attributed to the removal of In^{3+} from the complex by EDTA. As depicted in Fig. S14, the emission intensity ratio (I_{480nm}/I_{420nm}) of **R** went through from a higher level to a lower level after the successive addition of In^{3+} and EDTA, fluorescence intensity is recoverable despite a slight loss of fluorescence.

Application of R in Real Water Samples

The content variations of In^{3+} in tap water were measured using suggested fluorescence techniques to determine the practicability of **R**. With the addition of varied doses of In^{3+}, the linear fluorescence response of **R** was seen (Fig. S15). As displayed in Table S1, the indium ion content was accurately identified with suitable recovery rates (97.27–102.93%), and the relative standard deviation (RSD) of four measurements was less than 1.13%, showing that a satisfactory agreement of target ions was obtained. Based on these findings, **R** might be used as a practical tool to identify In^{3+} quantitatively in real-world water samples. In addition, **R** also showed good results for Pb^{2+} in tap water. As shown in Table S2, **R** was accurate in the determination of Pb^{2+} in tap water, with suitable recoveries (98.13 ~ 102.14%), and the relative deviations were less than 1.73%, indicating that the results of **R** were calibrated accurately for the determination of Pb^{2+}.

Conclusions

A ratiometric Schiff base fluorescent sensor **R** was designed and synthesized using ethyl 3-aminobenzo[b] thiophene-2-carboxylate as the parent compound. **R** exhibited an efficient ratiometric response to In^{3+} in MDF/H_2O tris buffer solution with a detection limit of 8.36×10^{-9} M. It was important that **R** could distinguish In^{3+} from Al^{3+} and Ga^{3+}. The possible complexation modes of **R** with In^{3+} were proposed based on job`s plot and ESI–MS spectrum, and the sensing mechanism of **R** for In^{3+} was rationalized by PET and ICT processes based on DFT calculations. Besides, **R** had potential application for quantitative detection of In^{3+} in tap water. In addition, **R** identified Pb^{2+} in a ratiometric response through a colorimetric response with a detection limit of 8.3×10^{-9} M.

Supplementary Information The online version contains supplementary material available at https://doi.org/10.1007/s10895-023-03576-7.

Author Contributions Shifeng Zhu: Writing – original draft, Writing – review & editing, Data curation, Formal Analysis, Methodology, Software, Validation. Liangru, Yang: Project administration , Funding acquisition, Supervision. Yingying Zhao: Writing – review & editing, Supervision, Software, Resources, Project administration, Methodology, Investigation, Funding acquisition, Conceptualization.

Funding The authors would like to acknowledge the financial support of the Doctor Foundation of Henan University of Technology (No. 2019BS058), the Key Science and Technology Project of Henan Province, China (No. 232102310027), the National Natural Science Foundation of China (21773056) and the Key Science and Technology Program of Henan Province (212102210608).

Data Availability No datasets were generated or analysed during the current study.

Declarations

Ethical Approval Not applicable.

Competing Interests The authors declare no competing interests.

References

1. Cho H, Chae JB, Kim C (2018) A thiophene-based blue-fluorescent emitting chemosensor for detecting indium (III) ion. Inorg Chem Commun 97:171–175. https://doi.org/10.1016/j.inoche.2018.09.037
2. Gökçeli G, Karatepe N (2021) Investigation of hydrogen post-treatment effect on surface and optoelectronic properties of indium tin oxide thin films. J Alloysd Compd 851. https://doi.org/10.1016/j.jallcom.2020.156861
3. Kho Y-M, Shin E (2017) Spiropyran-isoquinoline dyad as a dual chemosensor for Co(II) and In(III) detection. Molecules 22. https://doi.org/10.3390/molecules22091569
4. Pradhan D, Panda S, Sukla LB (2017) Recent advances in indium metallurgy: A review. Miner Process Extract Metal Rev 39:167–180. https://doi.org/10.1080/08827508.2017.1399887
5. Liu Y-H, Shaheen SM, Rinklebe J, Hseu Z-Y (2021) Pedogeochemical distribution of gallium, indium and thallium, their potential availability and associated risk in highly-weathered soil profiles of Taiwan. Environ Res 197. https://doi.org/10.1016/j.envres.2021.110994
6. Zhang Y, Li B (2022) A multifunctional selective fluorescent chemosensor for detection of Ga^{3+}, In^{3+} and Fe^{3+} in different solvents. J Mol Struct 1250. https://doi.org/10.1016/j.molstruc.2021.131461
7. Zheng Q, Ding F, Hu X, Feng J, Shen J, He X (2021) ESIPT-based fluorescent probe for bioimaging and identification of group IIIA ions in live cells and zebrafish. Bioorg Chem 109. https://doi.org/10.1016/j.bioorg.2021.104746
8. Tsao Y-C, Fan H-Y, Luo J-CJ (2021) Case reports of indium lung disease in Taiwan. J Formos Med Assoc 120:893–898. https://doi.org/10.1016/j.jfma.2020.08.009
9. Lee SC, Kim C (2020) A thiourea-naphthol based turn-on fluorescent sensor for detecting In^{3+} and its application. Inorg Chem Commun 112. https://doi.org/10.1016/j.inoche.2019.107752
10. Bomhard EM (2018) The toxicology of indium oxide. Environ Toxicol Pharmacol 58:250–258. https://doi.org/10.1016/j.etap.2018.02.003
11. Hamaguchi T, Omae K, Takebayashi T, Kikuchi Y, Yoshioka N, Nishiwaki Y, Tanaka A, Hirata M, Taguchi O, Chonan T (2008) Exposure to hardly soluble indium compounds in ITO production and recycling plants is a new risk for interstitial lung damage. Occup Environ Med 65:51–55. https://doi.org/10.1136/oem.2006.029124
12. Han DY, Kim JM, Kim J, Jung HS, Lee YH, Zhang JF, Kim JS (2010) ESIPT-based anthraquinonylcalix[4]crown chemosensor for In^{3+}. Tetrahedron Lett 51:1947–1951. https://doi.org/10.1016/j.tetlet.2010.02.006
13. Anbu Durai W, Ramu A, Dhakshinamoorthy A (2021) A Visual and ratiometric chemosensor using thiophene functionalized

hydrazone for the selective sensing of Pb^{2+} and F^- ions. J Fluoresc 31:465–474. https://doi.org/10.1007/s10895-020-02673-1
14. Sun T, Niu Q, Guo Z, Li T (2017) A simple highly sensitive and selective turn-on fluorescent chemosensor for the recognition of Pb^{2+}. Tetrahedron Lett 58:252–256. https://doi.org/10.1016/j.tetlet.2016.12.022
15. Walraven N, Bakker M, van Os B, Klaver G, Middelburg J, Davies G (2016) Pollution and oral bioaccessibility of Pb in soils of villages and cities with a long habitation history. Int J Environ Res Publ Health 13. https://doi.org/10.3390/ijerph13020221
16. Wan J, Zhang K, Li C, Li Y, Niu S (2017) A novel fluorescent chemosensor based on a rhodamine 6G derivative for the detection of Pb^{2+} ion. Sens Actuators B: Chem 246:696–702. https://doi.org/10.1016/j.snb.2017.02.126
17. Bhatt KD, Shah HD, Panchal M (2017) A switch-off fluorescence probe towards Pb(II) and Cu(II) ions based on a calix[4]pyrrole bearing amino-quinoline group. Luminescence 32:1398–1404. https://doi.org/10.1002/bio.3336
18. Liu Z, Jin W, Wang F, Li T, Nie J, Xiao W, Zhang Q, Zhang Y (2019) Ratiometric fluorescent sensing of Pb^{2+} and Hg^{2+} with two types of carbon dot nanohybrids synthesized from the same biomass. Sens Actuators B: Chem 296. https://doi.org/10.1016/j.snb.2019.126698
19. Arslan Y, Kendüzler E, Ataman OY (2011) Indium determination using slotted quartz tube-atom trap-flame atomic absorption spectrometry and interference studies. Talanta 85:1786–1791. https://doi.org/10.1016/j.talanta.2011.07.006
20. Kazemi E, Shokoufi N, Shemirani F (2011) Indium determination and preconcentration using fiber optic linear array detection spectrometry combined with dispersive liquid-liquid micro extraction. J Anal Chem 66:924–929. https://doi.org/10.1134/s1061934811100078
21. Tehrani MH, Companys E, Dago A, Puy J, Galceran J (2018) Free indium concentration determined with AGNES. Sci Total Environ 612:269–275. https://doi.org/10.1016/j.scitotenv.2017.08.200
22. Zu W, Yang Y, Wang Y, Yang X, Liu C, Ren M (2018) Rapid determination of indium in water samples using a portable solution cathode glow discharge-atomic emission spectrometer. Microchem J 137:266–271. https://doi.org/10.1016/j.microc.2017.11.001
23. Li B, Mei H, Wang M, Gu X, Hao J, Xie X, Xu K (2021) A near-infrared fluorescent probe for imaging of endogenous hydrogen sulfide in living cells and mice. Dyes Pigm 189. https://doi.org/10.1016/j.dyepig.2021.109231
24. Shi J, Zhang Z (2020) Synthesis and biological application of a water-soluble fluorescent probe for Fe^{3+} based on sodium benzo[c]chromene-2-sulfonate. Inorg Chim Acta 511. https://doi.org/10.1016/j.ica.2020.119790
25. Xing Y, Liu Z, Li B, Li L, Yang X, Zhang G (2021) The contrastive study of two thiophene-derived symmetrical Schiff bases as fluorescence sensors for Ga^{3+} detection. Sens Actuators B: Chem 347. https://doi.org/10.1016/j.snb.2021.130497
26. Xu Y, Yuan S, Zhang Y, Wang H, Yang X, Pei M, Zhang G (2020) A new multifunctional sensor for sequential recognizing of Zn^{2+} and PPi in acetonitrile solution and detection of In^{3+} in DMF solution. J Photochem Photobiol A Chem 392. https://doi.org/10.1016/j.jphotochem.2019.112348
27. Xu Y, Zhao S, Zhang Y, Wang H, Yang X, Pei M, Zhang G (2020) A selective "turn-on" sensor for recognizing In^{3+} and Zn^{2+} in respective systems based on imidazo [2,1-Whiazole. Photochem Photobiol Sci 19:289–298. https://doi.org/10.1039/c9pp00408d
28. Goshisht MK, Patra GK, Tripathi N (2022) Fluorescent Schiff base sensors as a versatile tool for metal ion detection: strategies, mechanistic insights, and applications. Mater Adv 3:2612–2669. https://doi.org/10.1039/d1ma01175h
29. Xing Y, Liu Z, Xu Y, Wang H, Li L, Li B, Yang X, Pei M, Zhang G (2020) Double Schiff base from thiophene-2,5-dicarboxylic acid as an "off–on–off" fluorescence sensor for the sequential detection of In^{3+} and PPi. New J Chem 44:13875–13881. https://doi.org/10.1039/d0nj03076g
30. Li Y, Niu Q, Wei T, Li T (2019) Novel thiophene-based colorimetric and fluorescent turn-on sensor for highly sensitive and selective simultaneous detection of Al^{3+} and Zn^{2+} in water and food samples and its application in bioimaging. Anal Chim Acta 1049:196–212. https://doi.org/10.1016/j.aca.2018.10.043
31. Musikavanhu B, Muthusamy S, Zhu D, Xue Z, Yu Q, Chiyumba CN, Mack J, Nyokong T, Wang S, Zhao L (2022) A simple quinoline-thiophene Schiff base turn-off chemosensor for Hg^{2+} detection: spectroscopy, sensing properties and applications. Spectrochim Acta Part A: Mol Biomol Spectrosc 264. https://doi.org/10.1016/j.saa.2021.120338
32. Rha CJ, Lee H, Kim C (2020) Simultaneous detection of Cu^{2+} and Co^{2+} by a water-soluble carboxamide-based colorimetric chemosensor. ChemistrySelect 5:1103–1108. https://doi.org/10.1002/slct.201904318
33. Yin P, Niu Q, Wei T, Li T, Li Y, Yang Q (2020) A new thiophene-based dual functional chemosensor for ultrasensitive colorimetric detection of Cu^{2+} in aqueous solution and highly selective fluorimetric detection of Al^{3+} in living cells. J Photochem Photobiol A Chem 389. https://doi.org/10.1016/j.jphotochem.2019.112249
34. Jang HJ, Ahn HM, Kim MS, Kim C (2017) A highly selective colorimetric chemosensor for sequential detection of Fe^{3+} and pyrophosphate in aqueous solution. Tetrahedron 73:6624–6631. https://doi.org/10.1016/j.tet.2017.10.012
35. Dhanya TM, Krishnan A, Anjali Krishna G, Francis S, Aswathy PV, Augustine M, Shanty AA, Divya KM, Savitha DP, Mohanan PV (2023) A novel benzothiophene incorporated Schiff base acting as a "turn-on" sensor for the selective detection of Serine in organic medium. Bioorg Chem 136. https://doi.org/10.1016/j.bioorg.2023.106525
36. Kathiravan A, Manjunathan T, Ramasubramanian K, Gopinath P (2022) An efficient Turn-ON fluorescent probe for fluoride ions – Meticulous investigations and development of arduino microcomputer integrated smartphone device. J Mol Liq 345. https://doi.org/10.1016/j.molliq.2021.117042
37. Khan SA, Asiri AM (2017) Physicochemical properties of novel methyl 2-{(E)-[(2-hydroxynaphthalen-1-yl)methylidene] amino}-4,5,6,7-tetrahydro-1-benzothiophene-3-carboxylate as turn-off fluorometric chemosensor for detection Fe^{3+} ion. J Mol Liq 243:85–90. https://doi.org/10.1016/j.molliq.2017.07.054
38. Popczyk A, Cheret Y, El-Ghayoury A, Sahraoui B, Mysliwiec J (2020) Solvatochromic fluorophores based on thiophene derivatives for highly-precise water, alcohols and dangerous ions detection. Dyes Pigm 177. https://doi.org/10.1016/j.dyepig.2020.108300
39. Wang Z, Zhang Y, Yin J, Li M, Luo H, Yang Y, Xu X, Yong Q, Wang S (2020) An easily available camphor-derived ratiometric fluorescent probe with AIE feature for sequential Ga^{3+} and ATP sensing in a near-perfect aqueous media and its bio-imaging in living cells and mice. Sens Actuators B Chem 320. https://doi.org/10.1016/j.snb.2020.128249
40. Mehta PK, Hwang GW, Park J, Lee K-H (2018) Highly sensitive ratiometric fluorescent detection of indium(III) Using fluorescent probe based on phosphoserine as a receptor. Analytical Chemistry 90:11256–11264. https://doi.org/10.1021/acs.analchem.8b01440
41. Leonczak P, Gao L-J, Ramadori AT, Lescrinier E, Rozenski J, De Jonghe S, Herdewijn P (2014) Synthesis and structure-activity relationship studies of 2-(1,3,4-Oxadiazole-2(3H)-thione)-3-amino-5-arylthieno[2,3-b]pyridines as Inhibitors of DRAK2. ChemMedChem 9:2587–2601. https://doi.org/10.1002/cmdc.201402234
42. Sadhanala HK, Pagidi S, Gedanken A (2021) High quantum yield boron-doped carbon dots: a ratiometric fluorescent probe for highly selective and sensitive detection of Mg^{2+} ions. J Mater Chem C 9:1632–1640. https://doi.org/10.1039/d0tc05081d

43. Velmurugan K, Vickram R, Jipsa CV, Karthick R, Prabakaran G, Suresh S, Prabhu J, Velraj G, Tang L, Nandhakumar R (2021) Quinoline based reversible fluorescent probe for Pb^{2+}; applications in milk, bioimaging and INHIBIT molecular logic gate. Food Chem 348:129098. https://doi.org/10.1016/j.foodchem.2021.129098
44. Mujthaba Aatif A, Selva Kumar R, Joseph S, Vetriarasu V, Abdul Majeed S, Ashok Kumar SK (2023) Pyridinecarbohydrazide-based fluorescent chemosensor for In^{3+} ions and its applications in water samples, live cells, and zebrafish imaging. J Photochem Photobiol A: Chem 434. https://doi.org/10.1016/j.jphotochem.2022.114257
45. Lu T, Chen F (2012) Multiwfn: A multifunctional wavefunction analyzer. J Comput Chem 33:580–592. https://doi.org/10.1002/jcc.22885